Deep Surveys and Galaxies with the Aid of Simulations

A. Ptak & R. Griffiths
Carnegie Mellon University, Pittburgh, PA; ptak@astro.phys.cmu.edu

ABSTRACT

Most *AXAF* and *XMM* observations of deep surveys and starburst galaxies will result in a large number of individual sources being detected. In the case of galaxies, most of the sources will be "local" and diffuse emission will be present as well. For both cases, the *AXAF* observations will be photon-limited while the *XMM* observation will be confusion-limited. When the same field is observed with both satellites it would obviously be desirable have in place an analysis scheme that maximizes the science return and gives "the best of both worlds". The availability of the simulators SciSim and MARX motivates a solution in which source detection and spatial and spectral analysis are iterated, using simulation both in the analysis and for consistency checks. We have begun development of software that is being tuned towards the simulation and analysis *AXAF* and *XMM* data. We have emphasized automation through the use of TCL scripts to drive tools (generating input data for tools that are not command -line driven). Later development will include spatial modeling of diffuse flux and iterations of simulations to arrive at self-consistent solutions that result in simulations that resemble the actual *AXAF* and *XMM* observations.

1. Introduction

XMM will have the largest effective area, by far, of any X-ray telescope by the time it is launched. Most *XMM* observations, including both pointed observations and survey fields, will result in many objects with a large number of counts, yielding high quality spectra, images and light curves. However, in some cases confusion, where more than one source lies within one spatial resolution element (e.g., the FWHM of the mirror), will be a problem. This will certainly complicate the analysis. Similarly, as has been the case with *ASCA* and, to a lesser extent, *ROSAT*, diffuse emission may vary on spatial scales smaller than the spatial resolution of *XMM*. In this case, the dispersion of source flux from one region to another due to the PSF (point-spread function) must be taken into account.

In contrast, *AXAF* will have the best spatial resolution of any X-ray telescope. However, many *AXAF* observations will be photon-limited, meaning that the number of source photons, rather than the level of the background or confusion, will be the dominant factor determining the limiting flux and the signal-to-noise ratio (SNR) for a source in an observation. When the same field is observed by both *AXAF* and *XMM*, it would obviously be desirable to maximize the return

of both satellites, taking advantage of the spatial resolution of *AXAF* and the effective area of *XMM*. We have begun to investigate the possibility of using the *AXAF* simulator MARX and the *XMM* simulator SciSim (with some help from QuickSim), for this purpose. Briefly, we plan to model an observation by driving both simulators with *same* input criteria. In the best-case scenario, the model can be varied to find a maximum-likelihood set of source positions, fluxes, spectra, and spatial distributions (for diffuse components). The worst case scenario is that this will not be possible (e.g., the fitting process may be too slow or not well-behaved numerically), but the simulations will serve to provide sample data sets to help tune (other) analysis techniques. Below we discuss our methodology for two cases, a deep survey and a starburst galaxy.

2. Methodology

Our methodology is to 1) create scripts to generate point sources (for both deep surveys and starburst galaxies) and to model the expected diffuse flux semi-analytically (in the case of starburst galaxies), 2) convert these models to appropriate input to MARX and SciSim, 3) add the non-instrumental background and run detection and analysis algorithms on the output for each telescope separately, and then 4) perform analysis that takes the output of both simulators *simultaneously*. To date we have a working package that performs (crudely at least) steps 1-3. We have been emphasizing modularity so that real data can be substituted for simulated data, and better analysis packages (i.e., those under development at the *AXAF* Science Center and the *XMM* Science Survey Center) can be substituted for our analysis routines (in step 3), as they become available.

2.1. Source Generation

2.1.1. Point Sources

Our source generator produces a log(N)-log(S) flux distribution of sources (i.e., a power-law). The spatial distribution can be either uniform (for deep surveys) or generated to follow an input FITS image (for starburst galaxies, as discussed below). The spectrum of each source is chosen according to user-specified probabilities. In the case of deep surveys, spectra were selected such that they sum to the shape of the X-ray background. In the case of starburst galaxies, models representing typical X-ray binaries (absorbed power-law spectra with $\Gamma \sim 1.8$) and supernovae (kT $\sim$ 1 keV plasmas) were chosen. Scripts then generate the appropriate SciSim or MARX input.

2.2. Diffuse Flux

We modeled the diffuse flux as the combination of the following components (based on the results of *ASCA*, *ROSAT*, and *SAX* observations of starburst galaxies given in Bregman, Schulman, & Tomisaka [1995, ApJ, 439, 155], Read et al. [1997, MNRAS, 286, 626], Ptak et al. [1997, AJ, 1286, 113], and Persic et al. [1998, astro-ph/9809256]):

- A hot nuclear region with $N_H = 10^{22}$ cm^{-2}, kT = 7 keV, 1/3 solar abundances (see Persic et al.), $\sim$ 20% of the 0.5-2.0 keV flux, with a spatial extent following a double exponential with a scale of 40" along the minor axis and 10" along the major axis.
- Hot ISM along the disk of the galaxy (4' by 1'), with $N_H = 10^{21}$ cm^{-2}, kT = 1 keV, solar abundances, $\sim$ 30% of the 0.5-2.0 keV flux.
- A wind expanding along the minor axis with an opening angle of 60°, $N_H = 10^{21}$cm^{-2}, kT = 0.3 keV, 1/3 solar abundances, $\sim$ 10% of the 0.1-0.5 keV flux, starting at the minor axis edge and falling off as $r^{-2.5}$.

Noise was added to both intensities and the boundaries of the components for realism. Images were generated using this model in 6 bandpasses: 0.1-0.2 5 keV, 0.25-0.5 keV, 0.5-1.0 keV, 1.0-2.0 keV, 2.0-5.0 keV and 5.0-10.0 keV. These images were then used as input for MARX and QuickSim (at the time that this work was completed, SciSim did not support image input). As mentioned above, point sources representing X-ray binaries and SN were also modeled (using an image generated using the disk and nuclear components as the spatial distribution). The point-source flux distribution slope was chosen to be 2.0. The total 2-10 keV flux of the point sources and the diffuse flux were each chosen to be $\sim 5 \times 10^{-12}$ ergs s^{-1}. Note that only M82 has a flux near this level and scale (M82 is one of the nearest starburst, at a distance of $\sim$ 3.6 Mpc). This model is shown in Figure 1.

3. Deep Survey Simulations

Figures 2 and 3 show the results of simulating a deep field based on the Cagnoni et al. (1998, ApJ, 493, 54) log(N)-log(S) relation determined from *ASCA* data, extrapolated to a flux of $\sim 8.7 \times 10^{-15}$ ergs cm^{-2} s^{-1} at which point it saturated the X-ray background. Here confusion does not appear to be a problem although this may not continue to be the case when more realistic models are employed (we have begun work producing a model which is consistent with both *ROSAT* surveys in the 0.5-2.0 keV bandpass and *ASCA* and *SAX* surveys in the 2-10 keV bandpass).

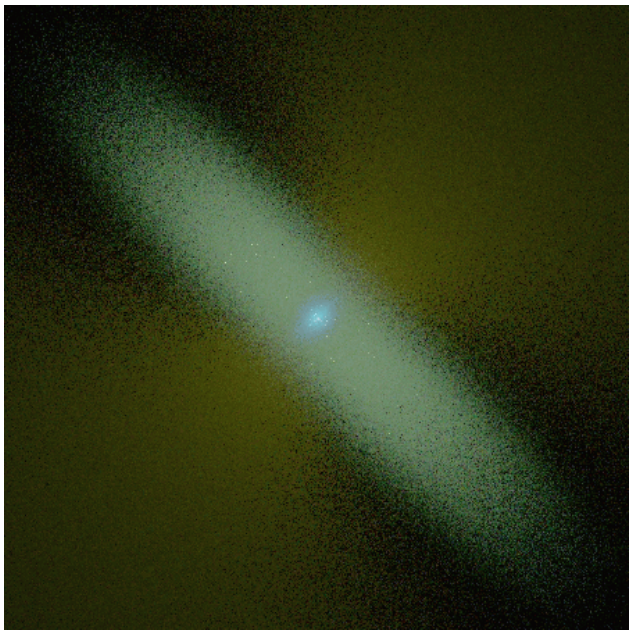

Fig. 1.— The starburst model used for the simulations. This image was created by combining the 0.1-0.5 keV, 0.5-2.0 keV and 2.0-10.0 keV images as red, green and blue, respectively. The image was scaled logarithmically in each bandpass.

4. Starburst Simulations

Figures 4-5 show the results of simulating the starburst model for *AXAF* and *XMM*. Note how the differences in the spectrum of the (extended) nuclear flux, diffuse disk flux, and several of the point sources can be inferred from the false-colors alone. Also the sensitivity of *AXAF* to point-source emission and *XMM* to diffuse emission is evident. Note that some of the "diffuse" flux is actually unresolved point-source emission, particularly in the case of the *XMM* simulation, in essence the extremal case of confusion.

5. Future Prospects

As stated above, we have been proceeding with refining our X-ray background (and starburst) models. We have already developed a radial profile fitting program that simultaneously fits multiple data sets and includes the PSF in the fitting process. This program will be expanded to perform true two-dimensional fitting of diffuse flux and also to explicitly fit for point sources. Finally, automation will be emphasized at all stages of the analysis to aid in the analysis of large data sets and in the determination of errors (i.e., with Monte Carlo techniques).

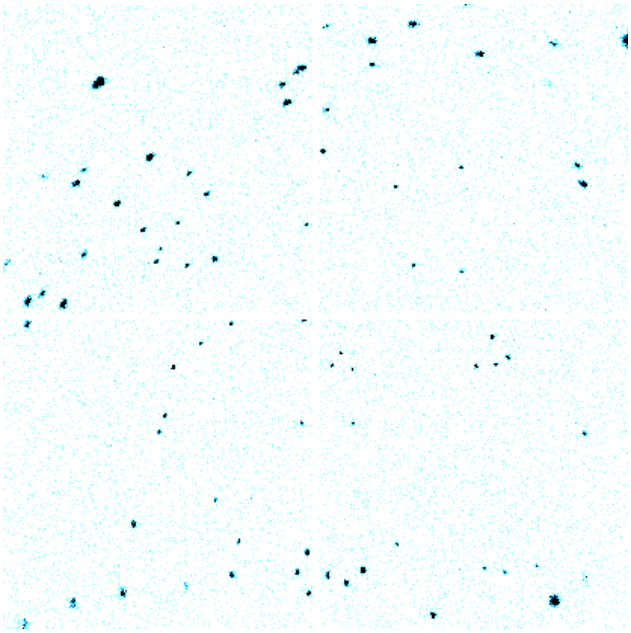

Fig. 2.— A 50 ks *AXAF* simulation of a deep field using MARX. An estimate of the non-X-ray background was added at a level of $\sim 1.2 \times 10^{-3}$ counts s^{-1} $arcmin^{-2}$ (note that this is probably overestimated somewhat since shielding was not included).

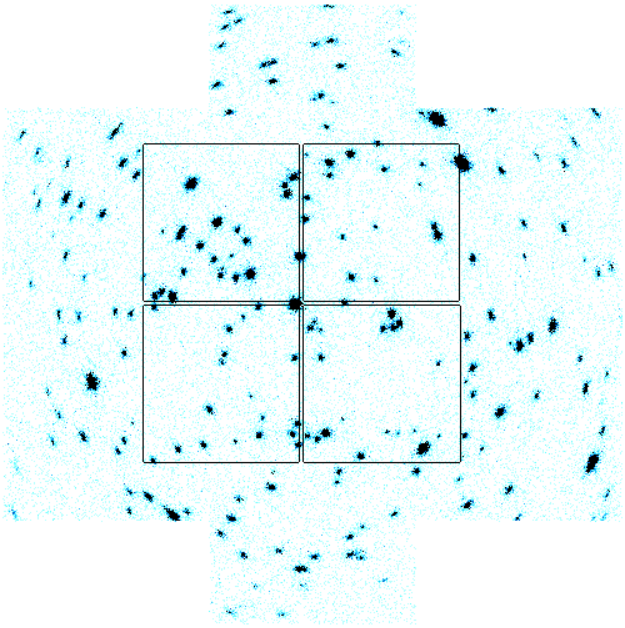

Fig. 3.— The same field as in Figure 2 as viewed by the *XMM* MOS using SciSim (a 100 ks simulation was performed since there are two MOS detectors). An estimate of the non-X-ray background was added at a level of $\sim 2.0 \times 10^{-4}$ counts s^{-1} $arcmin^{-2}$). The locations of the *AXAF* ACIS-I CCDs are shown.

Fig. 4.— A 100 ks *AXAF* ACIS-I simulation using the starburst model described in the text. This image is 10' by 10' and was created by combining the 0.1-0.5 keV, 0.5-2.0 keV and 2.0-10.0 keV images as red, green and blue, respectively. Each bandpass image was adaptively smoothed (to 10 counts per pixel with a maximum filter size of 50") and logarithmically scaled from 0.1-100 counts/pixel.

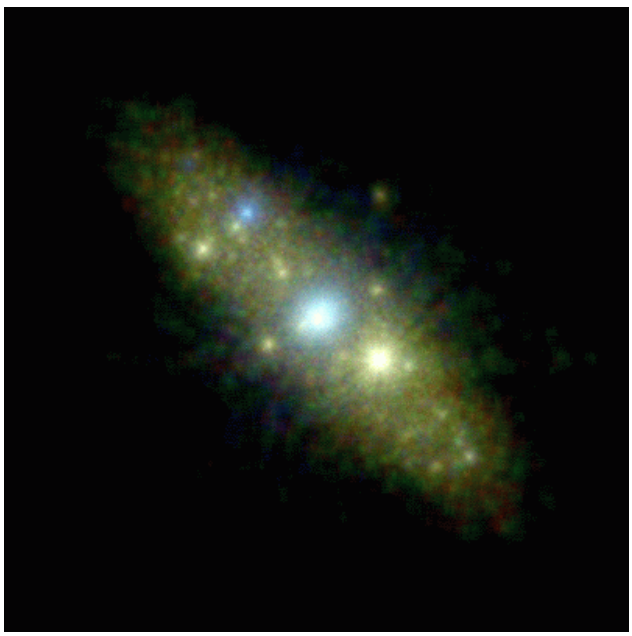

Fig. 5.— As in Figure 4 except for the *XMM* MOS detector. All parameters are the same except the field size is 13.4' by 13.4'.